IAHR AIRH

WORK GROUP ON

THE BEHAVIOR OF HYDRAULIC MACHINERY UNDER STEADY OSCILLATORY CONDITIONS

9th International Meeting, 7-9 September 1999, Brno, Czech Republic

WAVE SPEEDS AND PHASE VELOCITIES IN LIQUID-FILLED PIPES

D.J. Leslie & A.S. Tijsseling*

Abstract

Wave speeds and phase velocities play a crucial role in the theoretical description of the dynamic behaviour of liquid-filled pipes. Wave speeds describe propagating disturbances under transient conditions, whereas phase velocities describe wave trains under steady-oscillatory conditions. Except for linear non-dispersive systems, wave speeds and phase velocities are *not* the same.

This paper presents formulae and diagrams for wave speeds and phase velocities describing the axial, lateral and torsional vibration of liquid-filled pipes. Classical formulae are given. The influences of quasi-steady and unsteady fluid friction, viscous structural damping and fluid-structure interaction (FSI) are investigated. An apparent paradox resulting from time-domain and frequency-domain considerations is discussed.

This study aims at a deeper understanding of wave phenomena in pipe systems.

1. INTRODUCTION

The acoustic behaviour of liquid-filled pipes is determined by pressure waves in the liquid and stress waves (axial, lateral and torsional) in the pipes. Each type of wave has its own characteristic wave speed and phase velocity. Wave speeds are essential in a method of characteristics (MOC) time-domain analysis. They are the speeds of propagation of wave *fronts*. For the prismatic pipes considered herein, the wave speeds are constant. Phase velocities are basic in a harmonic frequency-domain analysis. They characterise wave *trains* and in general they are complex valued and frequency dependent.

This paper reviews the classical formulae for wave speeds and phase velocities and it investigates the influence on these of several viscous effects. The attenuation of wave fronts (jumps) is given by explicit formulae. The effect of fluid-structure interaction (FSI) on pressure and stress waves is shown in one illustrative chart.

For conciseness, many symbols are declared in Table 1 and in the nomenclature only.

1.1. Background

The present study is part of a project on modelling damping mechanisms in coupled liquid-pipe vibrations. Overviews of liquid-pipe coupling (FSI) and damping models are given in (Tijsseling 1996) and (Leslie and Tijsseling 1999) respectively.

---

*Department of Civil Engineering, University of Dundee, Dundee, DD1 4HN, UK.

Many theoretical FSI models lack proper damping mechanisms. This is not a limitation in the analysis of the initial phase of a transient vibration, which has been the focus of the authors' research so far. However, to widen the applicability of their models and software, the inclusion of damping mechanisms is prerequisite. Realistic models for liquid-pipe friction and for structural damping are needed: (i) to perform modal analyses and tests (natural frequencies and damping factors), (ii) to predict the steepness of wave fronts (an important parameter in FSI analyses) and (iii) to represent frequency-dependent behaviour (including visco-elasticity).

1.2. Test problem

A laboratory apparatus at Dundee University has been extensively used to study the effects of FSI on the transient (Vardy and Fan 1989) and free (Zhang *et al.* 1999) vibration of a closed, freely-suspended, liquid-filled pipe. Data for this particular pipe, given in Table 1, will be used for most of the calculations herein.

Table 1. Geometrical and material properties of Dundee single-pipe apparatus

Steel pipe		Water	
length:	$L = 4502$ mm	bulk modulus:	$K = 2.14$ GPa
inner radius:	$R = 26.01$ mm	mass density:	$\rho_f = 999$ kg/m^3
pipe wall thickness:	$e = 3.945$ mm	dynamic viscosity:	$\mu = 0.001$ Pa s
elastic modulus:	$E = 168$ GPa	area of flow:	$A_f = 2125$ mm^2
mass density:	$\rho_s = 7985$ kg/m^3		
Poisson's ratio:	$\nu = 0.29$		
shear coefficient:	$\kappa^2 = 0.53$		
area of pipe:	$A_s = 694$ mm^2		
second moment:	$I_s = 272900$ mm^4		

1.3. Basic equations

General forms of the basic equations describing one-dimensional linear wave propagation are:

$$\mathbf{A}\frac{\partial}{\partial t}\phi(z,t)+\mathbf{B}\frac{\partial}{\partial z}\phi(z,t)=\mathbf{r}(z,t)-\mathbf{C}\phi(z,t) \tag{1}$$

for the time-domain, and

$$s\mathbf{A}^*(s)\tilde{\phi}(z,s)+\mathbf{B}\frac{\partial}{\partial z}\tilde{\phi}(z,s)=\tilde{\mathbf{r}}(z,s)+\mathbf{A}\phi(z,0) \tag{2}$$

for the frequency-domain, in which $s = 2\pi i f$, $\tilde{}$ denotes a Laplace transformed variable and

$$\mathbf{A}^*(s)=\mathbf{A}+\frac{1}{s}\mathbf{C} \tag{3}$$

The state vector ϕ consists of generalised forces and *velocities*.

1.4. Wave speeds

In a method of characteristics (MOC) based time-domain (TD) approach, the wave speeds, denoted by c, are derived from the characteristic equation

$$\det(\mathbf{B} - \lambda\mathbf{A}) = 0 \tag{4}$$

in which no damping terms are included (they are within the **C** matrix and/or **r** vector). The wave speeds represent the constant propagation of contact discontinuities.

1.5. Phase velocities

In the frequency-domain (FD), spectral analysis produces phase velocities. These are denoted by $c(f)$ and are derived from the dispersion equation

$$\det\{\mathbf{B} - \lambda(s)\mathbf{A}^*(s)\} = 0 \tag{5}$$

Phase velocities are usually frequency-dependent and complex valued and wave trains may be expressed as

$$e^{i\omega\left(t - x/c(f)\right)} = e^{-qx} e^{i\omega\left(t - x/c_{eq}\right)} \tag{6}$$

where the complex phase velocity $c(f) = c_r + ic_i$ and $\omega = 2\pi f$. The equivalent wave speed c_{eq} and the attenuation factor q are real numbers defined by

$$c_{eq} = \frac{c_r^2 + c_i^2}{c_r} = \frac{|c(f)|^2}{c_r} \quad \text{and} \quad q = \frac{\omega c_i}{c_r^2 + c_i^2} = \frac{\omega c_i}{|c(f)|^2} \tag{7}$$

Note that the attenuation factor q is linearly increasing with ω, only if $c(f)$ is independent of ω.

2. TORSIONAL WAVES

The governing equations for torsional pipe motion are given by (1) with:

$$\mathbf{A} = \begin{pmatrix} 1 & 0 \\ 0 & -\dfrac{1}{GJ_s} \end{pmatrix}, \quad \mathbf{B} = \begin{pmatrix} 0 & -\dfrac{1}{\rho_s J_s} \\ 1 & 0 \end{pmatrix}, \quad \mathbf{C} = \begin{pmatrix} 0 & 0 \\ 0 & 0 \end{pmatrix}, \quad \boldsymbol{\phi} = \begin{pmatrix} \psi_{tor} \\ M_{tor} \end{pmatrix}, \quad \mathbf{r} = \begin{pmatrix} 0 \\ 0 \end{pmatrix} \tag{8}$$

in which M_{tor} is the torsional moment, ψ_{tor} is the angular velocity about the z-axis and J_s is the polar second moment of the pipe cross-section. Torsional pipe motion is assumed to be unaffected by the contained fluid. Hysteretic damping can be introduced by using a complex E (i.e. $E = E(1+i\eta)$), and hence G, modulus. It is noted that a complex G is meaningless in a MOC time-domain analysis. The characteristic and dispersion equations, (4) and (5) respectively, are identical because $\mathbf{C} = \mathbf{0}$ and hence $\mathbf{A} = \mathbf{A}^*$, so that the time- and frequency-domain analyses give the same result:

$$c_{tor} = c_{tor}(f) = \sqrt{G/\rho_s} \tag{9}$$

3. LATERAL WAVES

Timoshenko beam equations, including fluid mass and viscous structural damping (with respect to V and ψ and with damping coefficients denoted by D_S and D_B respectively, both with units Hz), describe lateral pipe motion. They are given by (1) with

$$\mathbf{A} = \begin{pmatrix} 1 & 0 & 0 & 0 \\ 0 & \dfrac{1}{\kappa^2 GA_s} & 0 & 0 \\ 0 & 0 & 1 & 0 \\ 0 & 0 & 0 & \dfrac{1}{EI_s} \end{pmatrix}, \quad \mathbf{B} = \begin{pmatrix} 0 & \dfrac{c_S^2}{\kappa^2 GA_s} & 0 & 0 \\ 1 & 0 & 0 & 0 \\ 0 & 0 & 0 & \dfrac{c_S^2}{EI_s} \\ 0 & 0 & 1 & 0 \end{pmatrix}, \quad \mathbf{C} = \begin{pmatrix} D_S & 0 & 0 & 0 \\ 0 & 0 & 1 & 0 \\ 0 & \dfrac{-c_S^2}{EI_s} & D_B & 0 \\ 0 & 0 & 0 & 0 \end{pmatrix}, \quad \boldsymbol{\phi} = \begin{pmatrix} V \\ Q \\ \psi \\ M \end{pmatrix}, \quad \mathbf{r} = 0 \tag{10}$$

The flexural wave speeds (TD) are defined as

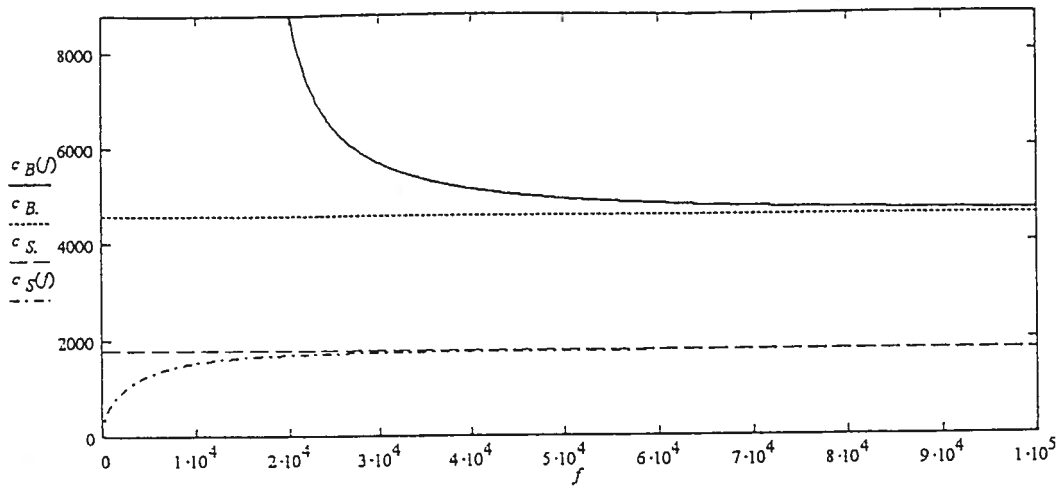

Figure 1: Lateral waves: phase velocities (in m/s) as function of frequency (in Hz) based on data in Table 1.

$$c_S = \sqrt{\kappa^2 G A_s \Big/ \left(\rho_s A_s + \rho_f A_f\right)} \quad \text{and} \quad c_B = \sqrt{E/\rho_s} \tag{11}$$

The phase velocities (FD) derived from the dispersion equation (5) are

$$c_S(f) = \sqrt{\frac{\left(\left(1+\frac{D_S}{2\pi i f}\right)c_S^2 + \left(1+\frac{D_B}{2\pi i f}\right)c_B^2\right) - \left\{\left(\left(1+\frac{D_S}{2\pi i f}\right)c_S^2 - \left(1+\frac{D_B}{2\pi i f}\right)c_B^2\right)^2 + 4\left(f_c/f\right)^2\left(1+\frac{D_S}{2\pi i f}\right)c_S^2 c_B^2\right\}^{1/2}}{2\left\{\left(1+\frac{D_S}{2\pi i f}\right)\left[\left(1+\frac{D_B}{2\pi i f}\right) - \left(f_c/f\right)^2\right]\right\}}}$$

$$c_B(f) = \sqrt{\frac{\left(\left(1+\frac{D_S}{2\pi i f}\right)c_S^2 + \left(1+\frac{D_B}{2\pi i f}\right)c_B^2\right) + \left\{\left(\left(1+\frac{D_S}{2\pi i f}\right)c_S^2 - \left(1+\frac{D_B}{2\pi i f}\right)c_B^2\right)^2 + 4\left(f_c/f\right)^2\left(1+\frac{D_S}{2\pi i f}\right)c_S^2 c_B^2\right\}^{1/2}}{2\left\{\left(1+\frac{D_S}{2\pi i f}\right)\left[\left(1+\frac{D_B}{2\pi i f}\right) - \left(f_c/f\right)^2\right]\right\}}} \tag{12}$$

where $f_c = (2\pi)^{-1}\sqrt{\kappa^2 G A_s/\rho_s I_s}$. In the low-frequency limit $f \downarrow 0$ the phase velocities $c_S(f)$ and $c_B(f)$, given by (12), both tend to zero. This is true with and without the damping terms included.

Figure 1 depicts the phase velocities, given by (12), as a function of the frequency of vibration. Damping effects have been neglected (i.e. $D_S = D_B = 0$). The velocities $c_B(f)$ are then purely imaginary for $f < f_c$, thus a second mode of vibration exists only at frequencies higher than f_c, the cut-on frequency. This is shown in Figure 1, with $c_B(f)$ emerging from the top of the graph for sufficiently large frequencies. From (12) it is seen that the phase velocity $c_B(f)$ tends to infinity as $f \downarrow f_c$. This phenomenon is an apparent paradox if $c_B(f)$ is thought of as a propagating wave *front* which has, as illustrated below, a finite speed c_B. With non-zero viscous damping coefficients the phase velocities are complex numbers, but neither are purely imaginary except for $c_B(f)$ at a critical value of the frequency giving an infinite equivalent wave speed (this does not occur at $f = f_c$ as previously defined but at $f = f_c(D_S, D_B)$ and does not always exist).

The high-frequency asymptotes in Figure 1 are the wave speeds c_S and c_B of (contact) discontinuities in shear force and bending moment, respectively. These are relevant in impact mechanics (see Flügge 1942 and Leonard and Budiansky 1954). Figure 2, an example with $c_S/c_B = 5^{-1}$, demonstrates both the propagation of discontinuities and the effects of frequency dispersion. The pipe of 20m length is subjected to a step moment of 200kNm on the right end. Responses are calculated at the instants $t_1 = (1/3)L/c_B$, $t_2 = (2/3)L/c_B$ and $t_3 = L/c_B$. The jump in the bending moment (top Fig.2) decreases as the front travels to the left. This is due to numerical error, as theoretically it should remain equal to the initial value (200kNm) when damping is

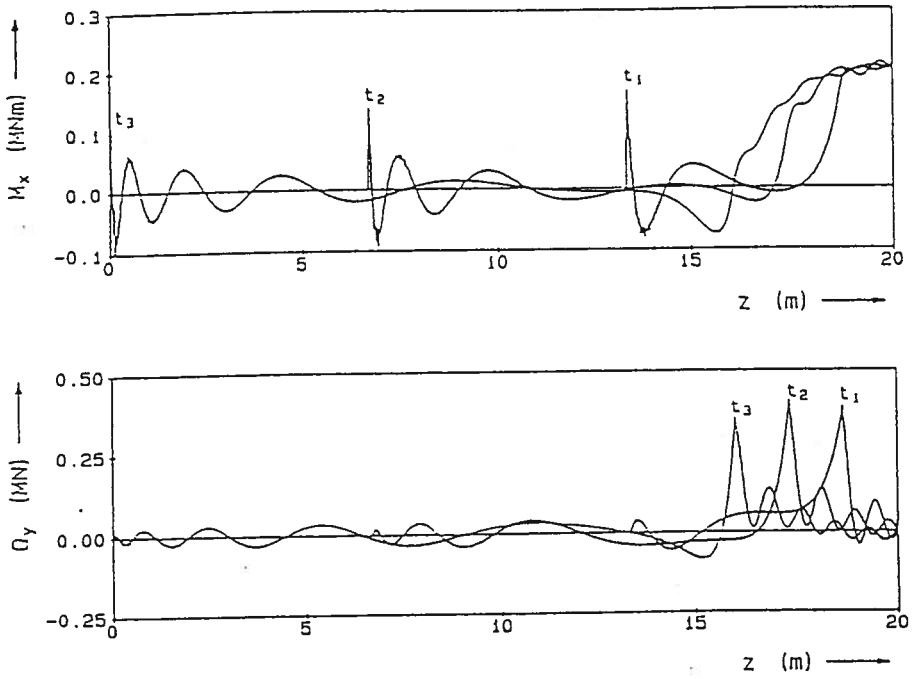

Figure 2: Propagation of discontinuity in bending moment M and associated shear force Q along pipe (calculated with MOC procedure not for the present test problem, but for example with c_S = 1031 m/s and c_B = 5156 m/s and without viscous structural damping); from Tijsseling 1993, p. 122.

neglected.

Behind the wave front dispersion occurs because of strong interaction between shear and bending waves. The jump will however decrease as its front travels when damping mechanisms are included. This decrease is governed by the relationship

$$(\delta M)_t = (\delta M)_0 e^{-\frac{1}{2}D_B t} \tag{13}$$

between the initial jump $(\delta M)_0$ and the jump at time t, $(\delta M)_t$. The wave front travels at constant speed with attenuation predicted by the new equation (13). It is also noted that the bending wave front travels with the speed of an *axial* stress wave (see Section 4.2) as might be expected, since bending is composed of axial stresses.

The shear wave front is illustrated in Figure 2 (bottom) as a peak in the shear force travelling to the left at speed c_S = 1031m/s.

Introducing a complex E, and hence G, modulus is a method by which hysteretic damping may be included within the equations (Cremer et al. 1988, pp. 195-204). This has meaning only in a frequency domain analysis and it has a similar effect on the phase velocities as introducing viscous damping by removing infinite equivalent wave speeds (i.e. purely imaginary bending phase velocities) except at a single frequency, $f = f_c(\eta)$.

4. AXIAL WAVES

4.1. Pressure waves

4.1.1. Quasi-steady linear friction

The waterhammer equations with a linear friction term are given by (1) with

$$\mathbf{A} = \begin{pmatrix} 1 & 0 \\ 0 & \dfrac{1}{\rho_f {c_f}^2} \end{pmatrix}, \quad \mathbf{B} = \begin{pmatrix} 0 & \dfrac{1}{\rho_f} \\ 1 & 0 \end{pmatrix}, \quad \mathbf{C} = \begin{pmatrix} f^* & 0 \\ 0 & 0 \end{pmatrix}, \quad \boldsymbol{\phi} = \begin{pmatrix} U_f \\ P \end{pmatrix}, \quad \mathbf{r} = \begin{pmatrix} 0 \\ 0 \end{pmatrix} \tag{14}$$

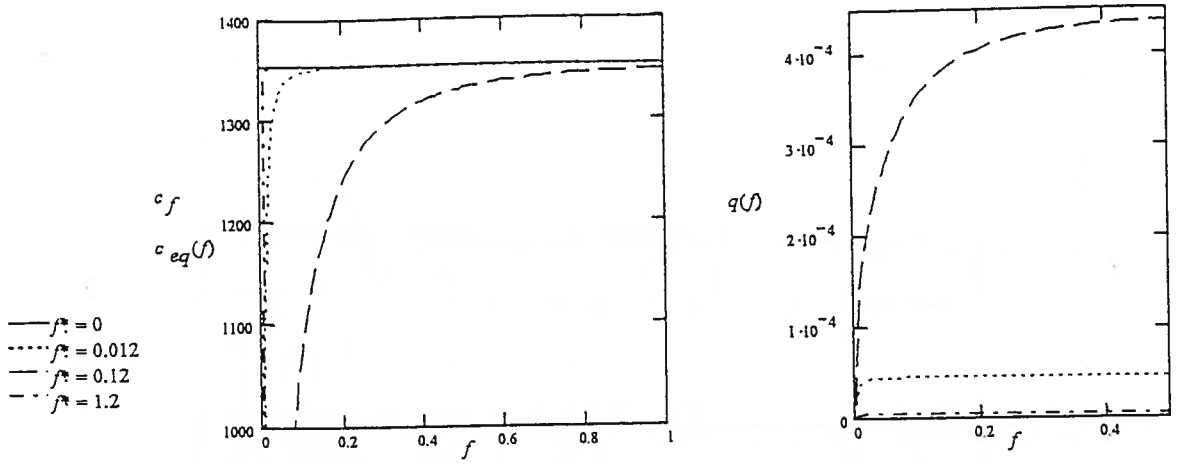

Figure 3: (Quasi-steady linear friction) Pressure waves: equivalent wave speeds (left, in m/s) and attenuation factors (right, in 1/m) as function of frequency (in Hz) based on data in Table 1.

(Wylie and Streeter 1993). Linear friction has been introduced through the term f^*U_f in which the value of f^* depends on the type of flow, namely: $f^*=8\mu/\rho_f R^2$ for laminar flow and $f^*=fU_0/2R$ for turbulent flow, where f is the Darcy-Weisbach friction coefficient and U_0 is the steady-state fluid velocity. The classical pressure wave speed (TD) is defined as

$$c_f = \sqrt{\left\{\frac{K}{\rho_f}\right\} \Big/ \left\{1+\frac{2KR}{Ee}\right\}} \tag{15}$$

The relation between an initial jump $(\delta P)_0$ and its value $(\delta P)_t$ at time t is

$$(\delta P)_t = (\delta P)_0 e^{-\frac{1}{2}f^* t} \tag{16}$$

This equation is derived from the ordinary differential equations (ODE) obtained by MOC. The ODE is written for upper and lower sides of the characteristic path along which the jump propagates and a difference of the two equations is taken. This difference can be written in terms of δP only, by using the relation $\delta P = \rho c_f \delta U_f$ (Joukowsky formula). The resulting ODE for δP is then integrated to give the desired result. Equation (16) predicts the attenuation with time of the magnitude of the jump (which propagates with constant speed) as caused by linear friction. This is particularly important in long pipe-lines.

The phase velocities (FD) obtained from the dispersion equation (5) are

$$c_f(f) = c_f\left(1+\frac{f^*}{2\pi i f}\right)^{-1/2} \tag{17}$$

The phase velocities are illustrated in Figure 3, showing equivalent wave speeds and attenuation factors as a function of frequency (see equation (7)). The graph demonstrates that the attenuation becomes constant as frequency increases, which can also be proven analytically such that $\lim_{f\to\infty} q(f) = f^*/2c_f$.

4.1.2. Unsteady friction

This section examines the influence of unsteady friction models on equivalent wave speeds. In the basic waterhammer equation (Navier-Stokes) the effect of viscosity is included through the term: $1/r\,\partial/\partial r\left(r\mu\partial U_f(r)/\partial r\right)$, where r is the radial coordinate and $U_f(r)$ is the axial velocity profile. A Laplace transform of the equations of motion and continuity is taken to find analytical solutions in the frequency domain in terms of transfer matrices. The wall shear stress for each frequency is found to be linearly related to the axial flow acceleration.

For laminar flow the viscosity μ is constant, whereas for turbulent flow a viscosity *profile*

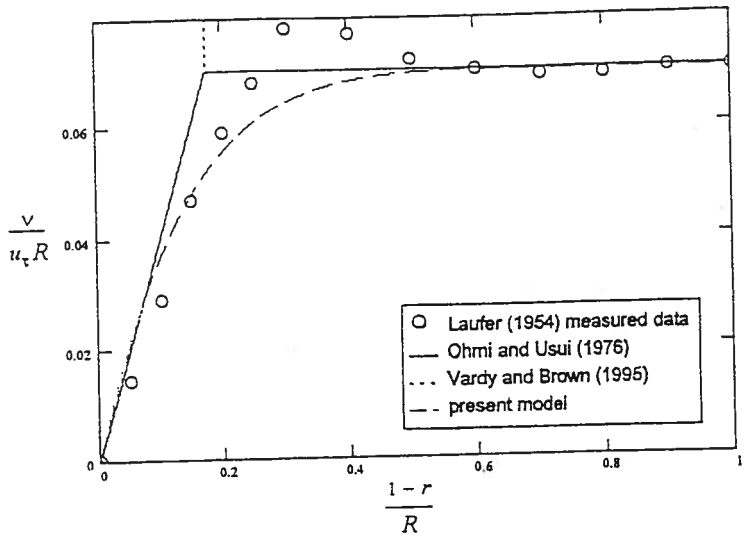

Figure 4: Viscosity profiles in steady turbulent pipe flow.

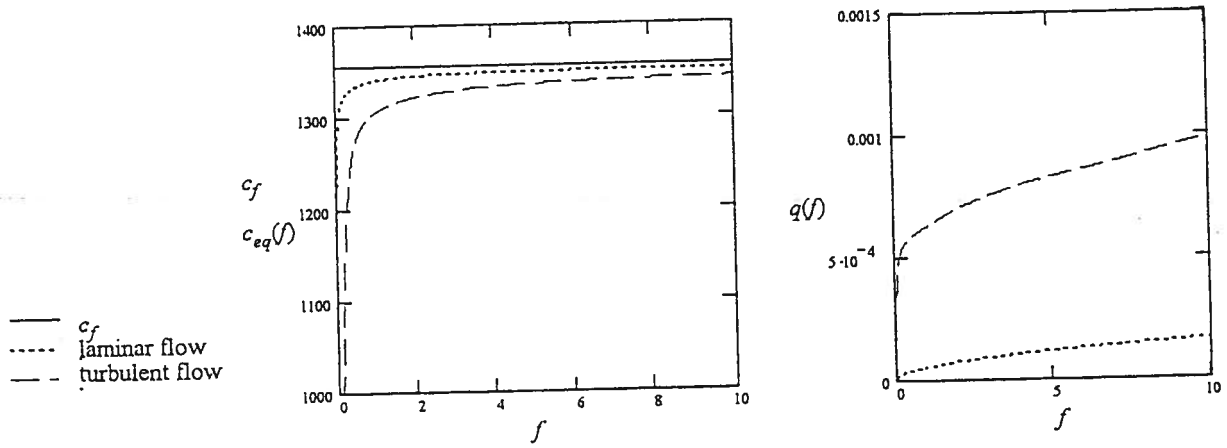

Figure 5: (Unsteady friction) Pressure waves: equivalent wave speeds (left, in m/s) and attenuation factors (right, in 1/m) as function of frequency (in Hz) based on data in Table 1.

is used in the analysis, i.e. the turbulent eddy viscosity depends on r. Exact models for laminar flow with unsteady friction may be found in Zielke 1968 (TD) and D'Souza and Oldenburger 1964 (FD). The turbulent flow model used herein is analogous to that of D'Souza and Oldenburger for laminar flow, which remains as a special case.

Including the aforementioned viscosity term in the basic equations leads to a complex frequency-dependent phase velocity which can be written in the form $c_f(f) = c_f / \{-i\beta(f)\}$ with, for laminar flow:

$$\beta(f) = \left[\frac{2}{i^{3/2} R(2\pi f/\nu)^{1/2}} \frac{J_1\left(i^{3/2} R(2\pi f/\nu)^{1/2}\right)}{J_0\left(i^{3/2} R(2\pi f/\nu)^{1/2}\right)} - 1 \right]^{-\frac{1}{2}} \tag{18}$$

in which J_0 and J_1 are Bessel functions and ν is the kinematic viscosity, and for turbulent flow:

$$\beta(f) = \left[\frac{2MD(R,f)}{D(R,f)} - 1 \right]^{-\frac{1}{2}} \tag{19}$$

in which $MD(r,f)$ and $D(r,f)$ are power series in terms of r, with frequency-dependent coefficients determined by the viscosity profile used (see Appendix). Laufer (1954) produced accurate

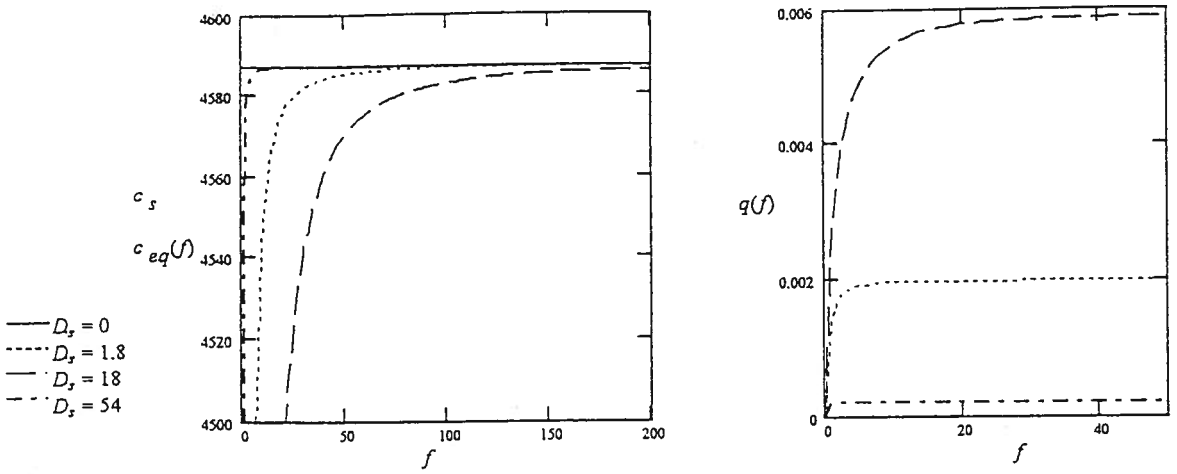

Figure 6: Axial stress waves: equivalent wave speeds (left, in m/s) and attenuation factors (right, in 1/m) as function of frequency (in Hz) based on data in Table 1.

experimental results for the turbulent viscosity profile in steady pipe flow. Using a viscosity profile of the form $\mu(r) = a+br^7$, the quantities a and b can be chosen to approximately fit Laufer's profile, as shown in Figure 4, where $a = \mu_c$ and $b = (\mu_w - \mu_c)/R^7$.

The quantity $R\sqrt{\omega/\nu_c}$, with ν_c the core kinematic viscosity and ω the angular frequency, is an important dimensionless number in this analysis. In the numerical calculations it restricts the range of values which may be used (in turbulent flows the ratio of core and wall viscosities, ν_c and ν_w, respectively, also affects the range). This is due to numerical errors and series failing to converge for large arguments. Approximations are available for the evaluation of Bessel functions with large arguments but not yet for the power series $MD(r,f)$ and $D(r,f)$ (given in the Appendix). In laminar flow, where ν is constant, and thus $\nu_c = \nu$, $R\sqrt{\omega/\nu_c}$ must be less than about 966, so that for the Dundee test pipe (Table 1) the numerical calculations are limited to frequencies less than 220Hz. For turbulent flow one is even restricted to frequencies less than 10Hz ($R\sqrt{\omega/\nu_c} \le 9.8$ when $\nu_c/\nu_w \approx 440$). With this restriction on frequencies and assuming a basic waterhammer frequency $4c_f/L$, the analysis is valid for pipelines longer than 30m (based on data in Table 1). Further approximations for both the Bessel functions and the power series $MD(r,f)$ and $D(r,f)$ with large arguments will extend the range of applicability of the model. Figure 5 compares equivalent wave speeds and attenuation factors for laminar and turbulent flows. It shows that for turbulent flow there is a higher attenuation and the equivalent wave speeds are reduced.

4.2. Stress waves

The beam equations for axial pipe vibration with viscous damping are given by (1) with

$$\mathbf{A} = \begin{pmatrix} 1 & 0 \\ 0 & \dfrac{-1}{\rho_s c_s^2} \end{pmatrix}, \quad \mathbf{B} = \begin{pmatrix} 0 & -1 \\ & \rho_s \\ 1 & 0 \end{pmatrix}, \quad \mathbf{C} = \begin{pmatrix} D_s & 0 \\ 0 & 0 \end{pmatrix}, \quad \boldsymbol{\phi} = \begin{pmatrix} U_s \\ \sigma \end{pmatrix}, \quad \mathbf{r} = \begin{pmatrix} 0 \\ 0 \end{pmatrix} \tag{20}$$

The classical wave speed (TD) is defined as

$$c_s = \sqrt{E/\rho_t} \tag{21}$$

The relation between an initial jump $(\delta\sigma)_0$ and its value $(\delta\sigma)_t$ at time t is

$$(\delta\sigma)_t = (\delta\sigma)_0 e^{-\frac{1}{2}D_s t} \tag{22}$$

Wave fronts travels at constant speed (21) with attenuation, as a result of viscous damping, predicted by (22). Equation (22) and its derivation are analogous to equation (16) for pressure

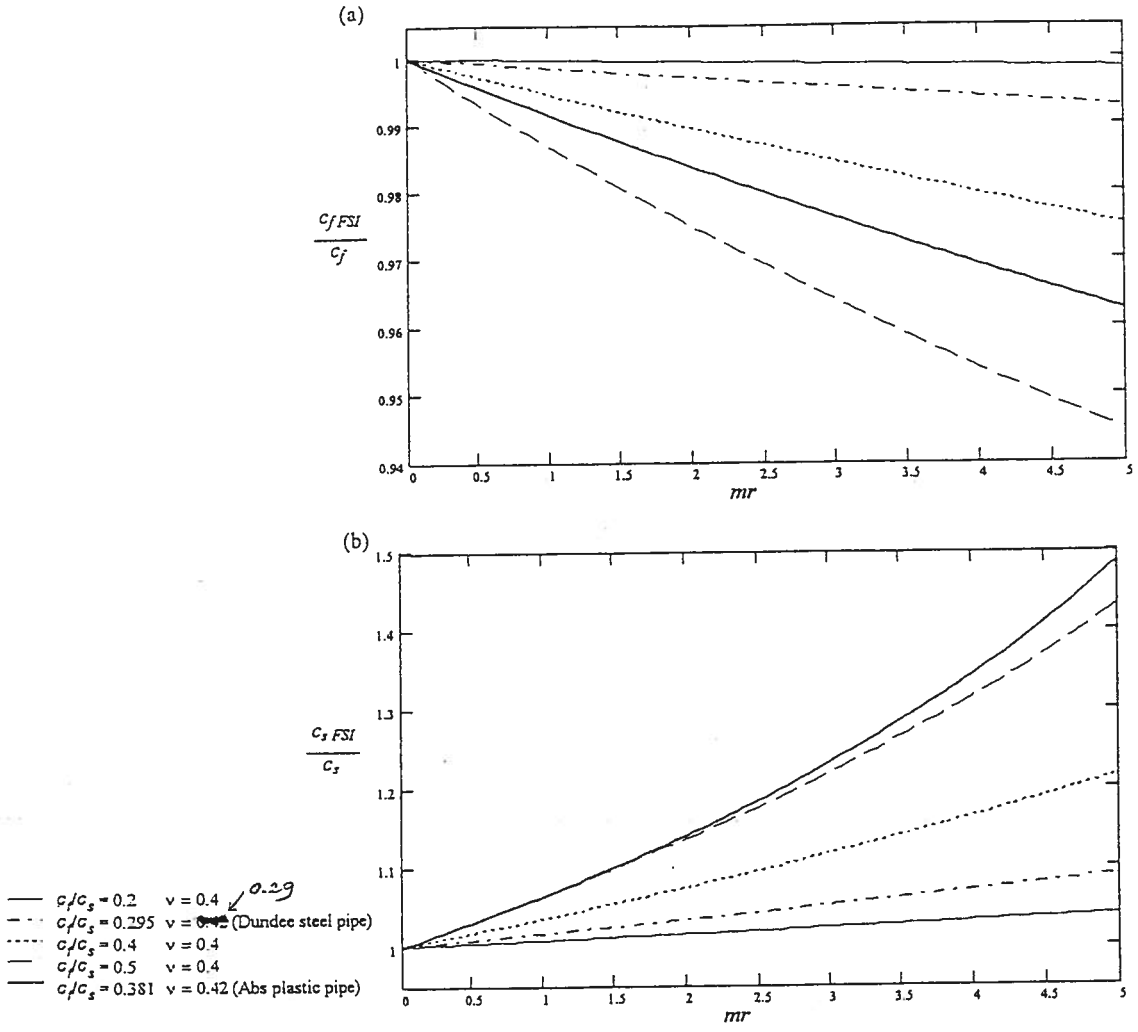

Figure 7: Graph of FSI/classical (a) pressure wave speed ratios and (b) stress wave speed ratios as function of mass ratio.

waves.

The phase velocity (FD) found from the dispersion equation (5) is

$$c_s(f) = c_s\left(1+\frac{D_s}{2\pi i f}\right)^{-1/2} \tag{23}$$

Figure 6 illustrates the phase velocities given by (23) in terms of equivalent wave speeds and attenuation factors as function of the frequency. It demonstrates that for large frequencies the equivalent wave speed asymptotes to c_s and the attenuation becomes constant. It can be proven that for large frequencies the attenuation asymptotes to $D_s/2c_s$.

4.3. FSI

Extended waterhammer and axial beam equations with linear friction coupling and structural viscous damping are given by (1) with

$$A=\begin{pmatrix} 1 & 0 & 0 & 0 \\ 0 & \frac{1}{\rho_f c_f^2} & 0 & 0 \\ 0 & 0 & 1 & 0 \\ 0 & \frac{\nu R}{E e} & 0 & \frac{-1}{\rho_s c_s^2} \end{pmatrix}, \quad B=\begin{pmatrix} 0 & \frac{1}{\rho_f} & 0 & 0 \\ 1 & 0 & -2\nu & 0 \\ 0 & 0 & 0 & \frac{-1}{\rho_s} \\ 0 & 0 & 1 & 0 \end{pmatrix}, \quad C=\begin{pmatrix} f_f & 0 & -f_f & 0 \\ 0 & 0 & 0 & 0 \\ -f_s & 0 & f_s+D_s & 0 \\ 0 & 0 & 0 & 0 \end{pmatrix}, \quad \phi=\begin{pmatrix} U_f \\ P \\ U_s \\ \sigma \end{pmatrix}, \quad r=0 \tag{24}$$

in which c_F is the classical wave speed given by

$$c_F = \sqrt{\left\{\frac{K}{\rho_f}\right\} \Big/ \left\{1+(1-\nu^2)\frac{2KR}{Ee}\right\}} \tag{25}$$

To focus on FSI effects ($\nu > 0$, where ν is Poisson's ratio) the damping mechanisms are neglected ($\mathbf{C} = \mathbf{0}$). Thus the wave speeds (TD) and phase velocities (FD) found from the characteristic and dispersion equations (4) and (5) are identical:

$$\begin{aligned} c_{f\,FSI} &= c_{f\,FSI}(f) = \sqrt{\frac{1}{2}\left\{\gamma^2 - \left(\gamma^4 - 4c_F{}^2 c_s{}^2\right)^{1/2}\right\}} \\ c_{s\,FSI} &= c_{s\,FSI}(f) = \sqrt{\frac{1}{2}\left\{\gamma^2 + \left(\gamma^4 - 4c_F{}^2 c_s{}^2\right)^{1/2}\right\}} \end{aligned} \tag{26}$$

where

$$\gamma^2 = \left(1+2\nu^2\frac{\rho_f}{\rho_t}\frac{R}{e}\right)c_F{}^2 + c_s{}^2 \tag{27}$$

The wave speeds, given by (26), are written in non-dimensional form to allow for a parameter study. In terms of the quantities ν, $mr = R\rho_f/2\rho_s e$ (the mass ratio between fluid and pipe) and the ratio c_f/c_s we have:

$$\begin{aligned} \frac{c_{f\,FSI}}{c_f} &= \sqrt{\frac{1+(c_f/c_s)^2 - \sqrt{\left(1+(c_f/c_s)^2\right)^2 - 4(c_f/c_s)^2\left(1-4\nu^2 mr\,(c_f/c_s)^2\right)}}{2(c_f/c_s)^2\left(1-4\nu^2 mr\,(c_f/c_s)^2\right)}}, \\ \frac{c_{s\,FSI}}{c_s} &= \sqrt{\frac{1+(c_f/c_s)^2 + \sqrt{\left(1+(c_f/c_s)^2\right)^2 - 4(c_f/c_s)^2\left(1-4\nu^2 mr\,(c_f/c_s)^2\right)}}{2(c_f/c_s)^2\left(1-4\nu^2 mr\,(c_f/c_s)^2\right)}} \end{aligned} \tag{28}$$

Note that c_f as defined in (15) has been used as a reference for $c_{f_{FSI}}$. Figure 7 shows that as the mass ratio mr increases so does the effect of FSI on the wave speeds: the pressure and stress wave speeds slightly decrease and increase, respectively, such that for smaller wave speed ratio c_f/c_s the influence of FSI becomes less.

5. CONCLUSIONS

When mechanical systems are non-dispersive and non-dissipative the wave speeds and phase velocities obtained from time- and frequency-domain analyses, respectively, are identical. For dispersive systems, e.g. laterally vibrating pipes, this is not true with wave speeds representing the constant propagation of contact discontinuities and frequency-dependent phase velocities describing oscillatory flow phenomena. From the phase velocities one can obtain equivalent wave speeds and attenuation factors.

With damping terms included in the analysis the equivalent wave speeds obtained are reduced compared to non-damped systems (attenuation factors increase) and this effect is more significant at lower frequencies. Damping has no effect on wave speeds in the time-domain analysis, because damping terms are not included in the characteristic equation and wave fronts therefore travel at constant speed. Attenuation of the travelling jump can be determined and for linear damping terms an exponential relationship can be obtained. FSI, however, does affect the wave speeds causing a change which depends on the fluid-structure mass ratio, Poisson's ratio and the ratio of the classical pressure and stress wave speeds.

Acknowledgements
This work has been part of a research project funded by the EPSRC under Grant number GR\M04501.

References

Tijsseling A.S. 1996 *Fluid-structure interaction in liquid-filled pipe systems: a review.* Journal of Fluids and Structures **10**(2), 109-146.

Leslie D.J. and Tijsseling A.S. 1999 *A review of modelling damping mechanisms in coupled liquid-pipe vibrations.* In Proc. of the 3rd ASME & JSME Joint Fluids Engineering Conf., San Francisco, USA, July 1999, Paper FEDSM99-6878.

Vardy A.E. and Fan D. 1989 *Flexural waves in a closed tube.* In Proceedings of the 6th International Conference on Pressure Surges, BHRA, Cambridge, UK, October 1989, 43-57.

Zhang L., Tijsseling A.S. and Vardy A.E. 1999 *FSI analysis of liquid-filled pipes.* Journal of Sound and Vibration **224**(1), 69-99.

Flügge W. 1942 *Die Ausbreitung von Biegungswellen in Stäben.* (*The propagation of bending waves in beams.*) (in German). Zeitschrift für angewandte Mathematik und Mechanik **22**, 312-318.

Leonard R.W. and Budiansky B. 1954 *On travelling waves in beams.* NACA TR 1173, Washington, USA.

Tijsseling A.S. 1993 *Fluid-structure interaction in case of waterhammer with cavitation.* Ph.D. Thesis, Delft University of Technology, Faculty of Civil Engineering, Communications on Hydraulic and Geotechnical Engineering, Report No. 93-6, ISSN 0169-6548, Delft, The Netherlands.

Cremer L., Heckl M. and Ungar E.E. 1988 *Structure-Borne Sound* (second edition). Berlin: Springer-Verlag.

Wylie E.B. and Streeter V.L. 1993 *Fluid transients in systems.* Englewood Cliffs, New Jersey, USA: Prentice Hall.

Zielke, W. 1968. *Frequency-dependent friction in transient pipe flow.* ASME Journal of Basic Engineering **90**, 109–115.

D'Souza A. F. and Oldenburger R. 1964. *Dynamic response of fluid lines.* ASME Journal of Basic Engineering **86**, 589–598.

Laufer J. 1954 *The structure of turbulence in fully developed pipe flow.* NACA TR 1174.

Ohmi N. and Usui T. 1976 *Pressure and velocity distributions in pulsating turbulent pipe flow.* Part 1:Theoretical treatments. Bulletin JSME **19**, 307-313.

Vardy A.E. and Brown J.M.B. 1995 *Transient, turbulent, smooth pipe friction.* IAHR Journal of Hydraulic Research **33**, 435-456.

Kuiken G.D.C. 1989 *Algorithms for the evaluation of Bessel functions of complex argument and integer order*. Appl. Math. Lett. 2(4), 353-356.

List of symbols (in addition to Table 1)

A, B, C	matrices of constant coefficients	f	frequency
A*	matrix given by (3)	f, f^*	friction coefficients
c	wave speed	G	shear modulus ($=\frac{1}{2}E/(1+\nu)$)
$c(f)$	phase velocity	J_s	polar second moment of area
D	damping coefficient	mr	fluid-structure mass ratio

M	bending moment
P	pressure
q	attenuation
Q	lateral shear force
r	vector
s	Laplace parameter
t	time
u_τ	friction velocity
U	axial velocity
V	lateral velocity
z	axial coordinate
$\beta(f)$	see (18) and (19)
γ	see (27)
δ	jump
ϕ	state vector
η	damping coefficient
λ	eigenvalue
ν	Poisson ratio, kinematic viscosity
ψ	angular velocity
ω	angular frequency

subscripts

B	bending
c	core
eq	equivalent
i	imaginary part
f, F	fluid
r	real part, radial coordinate
s	pipe (solid structure)
S	shear
tor	torsion
w	wall

abbreviations

FD	frequency domain
FSI	fluid-structure interaction
MOC	method of characteristics
ODE	ordinary differential equation
TD	time domain

Appendix

With a viscosity profile given by $\mu(r) = a+br^7$ the series $MD(r,f)$ and $D(r,f)$ in Eq.(19) are

$$MD(r,f) = \sum_{n=0}^{\infty} \frac{a_n r^n}{n+2} \quad \text{and} \quad D(r,f) = \sum_{n=0}^{\infty} a_n r^n \tag{A1}$$

where the frequency-dependent coefficients

$$a_0 = 1, \quad a_1 = 0,$$

$$a_n = \frac{i\omega\rho_f a_{n-2}}{an^2}, \quad n = 2,3,\ldots,6 \tag{A2}$$

$$a_n = \frac{i\omega\rho_f a_{n-2} - ba_{n-7}n(n-7)}{an^2}, \quad n = 7,8\ldots$$

define an analytical solution. Notice particularly that $a = \mu(0)$ is the core dynamic viscosity.

Bessel functions of order n, $J_n(z)$, are given by (or as above with $b = 0$)

$$J_n(z) = \sum_{k=0}^{\infty} \frac{(-1)^k \left(z/2\right)^{2k+n}}{k!(k+n)!} \tag{A3}$$

with approximations for moderate arguments given by Kuiken (1989) as:

$$J_n(z) = \begin{cases} \dfrac{1+(-1)^{n/2}\cos z}{2m} + \dfrac{1}{m}\displaystyle\sum_{k=1}^{m-1} \cos(z\sin t)\cos nt, & n = 0,2,\ldots \\ \dfrac{(-1)^{n-1/2}\sin z}{2m} + \dfrac{1}{m}\displaystyle\sum_{k=1}^{m-1} \sin(z\sin t)\sin nt, & n = 1,3,\ldots \end{cases} \tag{A4}$$

where

$$t = \frac{k\pi}{2m}, \qquad m \geq 2|z| + \tfrac{1}{4}\left(n + |\mathrm{Im} z|\right),$$

in which m is the number (integer) of intervals required for an absolute error less than 10^{-15}.

IAHR AIRH

WORK GROUP ON

THE BEHAVIOR OF HYDRAULIC MACHINERY UNDER STEADY OSCILLATORY CONDITIONS

9th International Meeting, 7-9 September 1999, Brno, Czech Republic

DISCUSSIONS

SESSION E – Hydroelastic vibrations in hydraulic turbines

PAPER E.1 – D.J.Leslie, A.S.Tijsseling:

WAVE SPEEDS AND PHASE VELOCITIES IN LIQUID-FILLED PIPES

Question from: H. Brekke:

I will congratulate you with an interesting paper, which is very complex. My question is very simple:

This theory is very complex and you have made computations of a simple system. Do you have any idea of how far is the future it will be possible to analyse complex piping systems of pipes connected in 3 dimensional space containing pipes of different stiffness (wall thickness)? Can you make a short comment on this?

Answer from: D. Leslie

Indeed, the underlying calculations are complex, but the final result is not. The final result is a frequency-dependent phase-velocity with a real and an imaginary part, which can be directly fed into conventional one-dimensional transfer matrix methods. These methods are widely used in practice to analyse industrial pipe systems.